

## Emergence of chaos in a spatially confined reactive system



Valérie Voorsluijs\*, Yannick De Decker

Nonlinear Physical Chemistry Unit and Center for Nonlinear Phenomena and Complex Systems (CENOLI), Université libre de Bruxelles (ULB), Campus Plaine, C.P. 231, B-1050 Brussels, Belgium

### HIGHLIGHTS

- A model of chemical chaos in a crowded system is investigated.
- The model is studied with deterministic and stochastic simulations.
- Molecular crowding generates absorbing states which can destroy chaos.
- Inhomogeneous fluctuations can transform chaos into regular oscillations.
- Diffusion and system size act as effective bifurcation parameters.

### ARTICLE INFO

#### Article history:

Received 5 January 2016  
Accepted 13 May 2016  
Available online 24 May 2016  
Communicated by Chennai Guest Editor

#### Keywords:

Chaos  
Stochastic  
Confinement  
Bifurcation

### ABSTRACT

In spatially restricted media, interactions between particles and local fluctuations of density can lead to important deviations of the dynamics from the unconfined, deterministic picture. In this context, we investigated how molecular crowding can affect the emergence of chaos in small reactive systems. We developed to this end an amended version of the Willamowski–Rössler model, where we account for the impenetrability of the reactive species. We analyzed the deterministic kinetics of this model and studied it with spatially-extended stochastic simulations in which the mobility of particles is included explicitly. We show that homogeneous fluctuations can lead to a destruction of chaos through a fluctuation-induced collision between chaotic trajectories and absorbing states. However, an interplay between the size of the system and the mobility of particles can counterbalance this effect so that chaos can indeed be found when particles diffuse slowly. This unexpected effect can be traced back to the emergence of spatial correlations which strongly affect the dynamics. The mobility of particles effectively acts as a new bifurcation parameter, enabling the system to switch from stationary states to absorbing states, oscillations or chaos.

© 2016 Elsevier B.V. All rights reserved.

### 1. Introduction

Nanosystems offer a wide range of applications in materials science, biology, medicine and catalysis. Polymeric or lipidic micelles are for example used as drug delivery vehicles and the geometry of the nanopores of zeolites allows one to improve the selectivity of chemical reactions [1]. The dynamics of reactions taking place in such small systems can reveal especially complex, as it emerges from the interplay between numerous effects. The small size of these structures induces the confinement of molecules, which can lead to changes in the mechanism and in the rate of the reactions, as compared to unconfined systems [2].

The interactions between adjacent particles and the fluctuations of particles densities can also lead to important deviations from the traditional mass action law [3–5].

In this context, the very possibility of observing *chaotic dynamics* at the nanoscale has been widely debated in the literature. It is well established that at a macroscopic level the traditional laws of chemical kinetics, despite their deterministic nature, can lead to a chaotic evolution of the concentrations in both time and space. However, reactions are intrinsically discrete events taking place with a given probability. The number of particles is thus a discrete and fluctuating quantity and the dynamics of reactive systems is expected to be affected by such fluctuations of internal origin. According to Fox and Keizer, in a chaotic system, fluctuations are amplified and are of the same order of magnitude as the variables of interest [6]. Chaos of deterministic origin should thus not be expected in small systems. In fact, the authors put forth the idea that the validity of the deterministic equations themselves

\* Corresponding author.

E-mail addresses: [vvoorslu@ulb.ac.be](mailto:vvoorslu@ulb.ac.be) (V. Voorsluijs), [ydedecke@ulb.ac.be](mailto:ydedecke@ulb.ac.be) (Y. De Decker).

becomes questionable. On the contrary, Nicolis et al. argued that the existence of an underlying (strange) attractor confers a certain robustness to deterministic chaos. The macroscopic laws would still be valid and would correctly predict the evolution of the most probable value of the variables [7]. As a consequence, a “blurred” form of deterministic chaos could be observed in systems subject to internal fluctuations.

This question has also been addressed with numerical simulations. For small well-stirred systems, chaos has been observed with Gillespie simulations of the master equation for the Willamowski–Rössler model [8], while it was seen to disappear totally in other instances [9]. It appears from these studies that the competition between the strange attractor and other attractors (like fixed points) plays an important role. Several studies also addressed the role of diffusion in the emergence of chaotic behaviors. Kapral and Wu used reactive lattice-gas automata to analyze the behavior of the Willamowski–Rössler [10,11] and of the autocatalator [12] models in the case of dilute systems. They concluded that chaos can indeed be observed when species diffuse sufficiently rapidly, and that the presence of fluctuations reflects itself under the form of dephasing and smoothing of the trajectories in phase space. For slowly diffusing molecules, destruction of phase coherence is observed and no form of structured chaos can be found.

None of the above works considered the role played by the molecular confinement that is characteristic of reactive nanosystems. However, it is well known that crowding effects in stochastic systems can result in the emergence of inhomogeneous fluctuations of composition that affect diffusion [13] and the chemical dynamics both quantitatively and qualitatively. Several reactive nonlinear behaviors have for example been studied on low-dimensional lattices :

1. the reversible reaction  $A + nX \rightleftharpoons (n + 1)X$  with  $n = 1$  and  $n = 2$  [14–16];
2. the Schlögl models I and II [17];
3. a lattice Lotka–Volterra model [18,19];
4. a modified lattice Lotka–Volterra model where one of the bimolecular reaction steps is replaced by a quadrimolecular process [20];
5. nonspatial and spatial individual level models describing prey–predator dynamics [21–23];
6. a Brusselator model with nonlocal interactions [24];
7. a population dynamics model involving four interacting species and exhibiting chaotic behavior in the macroscopic description [25].

The spatial restrictions induced by the substrate can lead to a displacement of stationary states [14,15,17,18] or to the disappearance of dynamical behaviors predicted by the deterministic description (such as bistability [17] and oscillations [18]). The dynamics of these systems is dominated by fluctuation-induced transitions to poisoning or absorbing states where some species are completely consumed, or in other cases, intrinsic fluctuations can give rise to coherent cyclic behaviors [22,23] or to traveling waves [24].

In this work, we investigate how confinement can affect the conclusions drawn on the existence of chaotic behaviors in fluctuating reactive systems. We develop to this end an amended version of the classical Willamowski–Rössler model [26] where we account for molecular crowding. This model is described in Section 2. In Section 3, we analyze the deterministic kinetics of this model. We focus in particular on the determination and on the linear stability analysis of the stationary states, and on the parametric conditions leading to deterministic chaos. Then, we study the influence of fluctuations with stochastic simulations (Section 4). We consider both the well-stirred limit and the role of diffusion. We show that because of the existence of

absorbing states, chaotic behaviors are destroyed for a wide range of parameters and system sizes for well-stirred systems. When the mobility of the species is low, chaos disappears as well because of a destruction of phase coherence similar to what has been reported earlier in the literature. However, and more surprisingly, we observe that chaos can reappear and that regular oscillations can be found for *intermediate* mobilities of the reactive species. In Section 5, we summarize the main conclusions of this study and possible future work is presented.

## 2. Extension of the Willamowski–Rössler model

The Willamowski–Rössler model is a thermodynamically consistent model for deterministic chaos in reactive systems. It involves 5 chemical reactions taking place in a well-stirred, ideal and isothermal system [26]:



The activities  $a_i$  of the species  $A_i$  are kept constant thanks to exchanges with external reservoirs (chemostats), in order to maintain the system out of equilibrium. Deterministic chaos can be observed for a wide range of parameters in this model. For example, in the simplifying limit where  $k_{-2} = k_{-3} = k_{-4} = 0$  and  $k_2 = k_4$  the deterministic evolution laws for the populations  $\chi_x$ ,  $\chi_y$  and  $\chi_z$

$$\frac{d\chi_x}{dt} = k_1 a_1 \chi_x - k_{-1} \chi_x^2 - k_2 \chi_x \chi_y - k_4 \chi_x \chi_z \quad (6)$$

$$\frac{d\chi_y}{dt} = k_2 \chi_x \chi_y - k_3 a_5 \chi_y \quad (7)$$

$$\frac{d\chi_z}{dt} = -k_4 \chi_x \chi_z + k_5 a_4 \chi_z - k_{-5} \chi_z^2, \quad (8)$$

lead to chaos through a succession of period doublings. This dynamics can be traced back to a saddle-focus configuration centered around one of the 6 possible steady states associated with Eqs. (6)–(8).

The Willamowski–Rössler model rests on the assumption that the reactions take place in an ideal (and thus a dilute) system. At high concentration however, molecular crowding is expected as a consequence of the finite size of the different molecules involved. To include such effects, we consider that the three species of interest  $X$ ,  $Y$  and  $Z$  are contained in a system having a finite, constant volume. We then divide space in a collection of boxes forming a regular discrete lattice. Each of these boxes can either be occupied by a single particle of  $X$ ,  $Y$  or  $Z$ , or be empty (we denote such empty boxes with the symbol  $S$ ). Consequently, the molar fractions of the different species of interest are connected at all times by a conservation rule:

$$x + y + z + s = 1, \quad (9)$$

where molar fractions are defined as the ratio between the number of boxes occupied by a species and the total number of boxes. The other reactants  $A_i$  are placed outside the volume of the reaction chamber and their activities are maintained constant like in the original Willamowski–Rössler model.

Because the volume of the system must remain constant at all times, and in order to comply with Eq. (9), the reactions (1)–(5) must be changed to



The first reaction now accounts for the fact that the creation of a particle X in the system can only take place if an empty space S is available. The destruction of a Y particle in reaction (13) frees an empty space in the system since  $A_2$  is outside the volume where spatial restrictions apply. The other reactions have been adapted in a similar fashion.

Adopting the same restricted set of parameters as what is done for the traditional Willamowski–Rössler model, the evolution equations for the molar fractions read

$$\frac{dx}{dt} = k_1 a_1 x s - k_{-1} x^2 - k_2 x y - k_4 x z \quad (15)$$

$$\frac{dy}{dt} = k_2 x y - k_3 a_5 y \quad (16)$$

$$\frac{dz}{dt} = -k_4 x z + k_5 a_4 z s - k_{-5} z^2. \quad (17)$$

These equations form a closed system because of the conservation rule (9). To reduce the number of parameters we introduce the adimensional time and constants

$$\begin{aligned} \tau &= k_3 a_1 t, & \alpha_1 &= \frac{k_1}{k_3}, \\ \alpha_{-1} &= \frac{k_{-1}}{k_2}, & \alpha_3 &= \frac{a_5}{a_1}, \\ \alpha_5 &= \frac{k_5 a_4}{k_3 a_1}, & \alpha_{-5} &= \frac{k_{-5}}{k_2} \end{aligned}$$

and we restrict ourselves to cases where  $k_2 = k_4 = k_3 a_1$ . The set of deterministic evolution laws that will be used in this work is consequently given by

$$\frac{dx}{d\tau} = \alpha_1 x (1 - x - y - z) - \alpha_{-1} x^2 - x y - x z \quad (18)$$

$$\frac{dy}{d\tau} = x y - \alpha_3 y \quad (19)$$

$$\frac{dz}{d\tau} = -x z + \alpha_5 z (1 - x - y - z) - \alpha_{-5} z^2. \quad (20)$$

Note that for dilute systems,  $x + y + z \ll 1$  and the above equations have the same structure as Eqs. (6)–(8), assuming that  $\alpha_5 \ll (1, \alpha_{-5})$ . In the next Section, we discuss the most prominent features of this amended Willamowski–Rössler model.

### 3. Deterministic behavior

As in the original Willamowski–Rössler model, the deterministic evolution equations (18)–(20) admit 6 stationary states:

$$St_1 \equiv (0, 0, 0)$$

$$St_2 \equiv \left( \frac{\alpha_1}{\alpha_1 + \alpha_{-1}}, 0, 0 \right)$$

$$St_3 \equiv \left( 0, 0, \frac{\alpha_5}{\alpha_5 + \alpha_{-5}} \right)$$

$$St_4 \equiv \left( \frac{\alpha_1 \alpha_{-5} - \alpha_5}{\alpha_{-1} \alpha_{-5} - \alpha_1 + \alpha_1 \alpha_{-5} - \alpha_5 + \alpha_{-1} \alpha_5 - 1}, 0, \frac{\alpha_{-1} \alpha_5 - \alpha_1}{\alpha_{-1} \alpha_{-5} - \alpha_1 + \alpha_1 \alpha_{-5} - \alpha_5 + \alpha_{-1} \alpha_5 - 1} \right)$$

$$St_5 \equiv \left( \alpha_3, \frac{\alpha_1 (1 - \alpha_3) - \alpha_{-1} \alpha_3}{\alpha_1 + 1}, 0 \right)$$

$$St_6 \equiv \left( \alpha_3, \frac{\alpha_1 \alpha_{-5} - \alpha_5 - \alpha_3 (\alpha_{-1} \alpha_{-5} - \alpha_1 + \alpha_1 \alpha_{-5} - \alpha_5 + \alpha_{-1} \alpha_5 - 1)}{\alpha_{-5} (1 + \alpha_1)}, \frac{\alpha_5 + \alpha_{-1} \alpha_3 \alpha_5 - \alpha_3 - \alpha_1 \alpha_3 - \alpha_3 \alpha_5}{\alpha_{-5} (1 + \alpha_1)} \right).$$

Except for  $St_6$ , the solutions represent “absorbing” states where at least one species is absent and cannot be generated anymore, since the corresponding production mechanisms are autocatalytic. States  $St_1$ ,  $St_2$  and  $St_3$  always exist and correspond to physically acceptable values for the steady state molar fractions. The stationary solutions for  $x$ ,  $y$  or  $z$  can become negative for some values of the parameters for  $St_4$ ,  $St_5$  and  $St_6$ , the existence of which is thus constrained to a subset of parameter space.

Linear stability analysis of these fixed points reveals that state  $St_1$ , which corresponds to an empty system, always has two positive and one negative real eigenvalues and is thus a saddle. State  $St_2$  is a stable node for  $\alpha_{-1} \alpha_5 \leq \alpha_1 \leq \alpha_{-1} \alpha_3 / (1 - \alpha_3)$  and is a saddle otherwise. A similar situation holds for state  $St_3$ , which is a stable node whenever  $\alpha_1 \leq \alpha_5 / \alpha_{-5}$  and a saddle whenever this inequality is not respected. State  $St_4$  behaves in the same way, but its region of stability is delimited by more intricate constraints acting on the parameters, the exact form of which is irrelevant for our purpose.

The analysis of states  $St_5$  and  $St_6$  reveals features that suggest a possible emergence of chaos. Depending on the choice of parameters,  $St_5$  is either a stable node, a saddle, a stable focus-node or a saddle-focus. State  $St_6$  can either be a stable node, a stable focus-node or a saddle-focus. As we discuss hereunder, the coexistence of two saddle-foci can lead, under certain conditions, to chaotic trajectories. We performed numerical integrations to analyze the nonlinear dynamical behavior of the system for conditions under which these states become unstable. These investigations revealed that state  $St_6$  plays a central role in the appearance of chaos. Keeping all parameters constant and varying  $\alpha_1$  from large to smaller values,  $St_6$  becomes unstable as it switches from a stable focus-node to a saddle-focus through a Hopf bifurcation, which leads to simple sustained oscillations. Figs. 1(a) and 2(a) depict time series and a power spectrum corresponding to such oscillations. Decreasing  $\alpha_1$  further leads to a period-doubling cascade and thus to multiperiodic oscillations of increasing complexity (as shown in Figs. 1(b) and (c)) that culminates in deterministic chaos (see Fig. 1(d)). The chaotic character of the dynamics can be confirmed in different ways. The associated power spectrum (Fig. 2(b)) is characterized by the coexistence of numerous incommensurate frequencies. Oscillations and chaos can also be easily distinguished in phase space in view of the fractal structure of the chaotic attractor (Fig. 3), which is characterized by a correlation dimension  $D_2 \approx 1.9$  (as calculated with the routines in Tisean 3.0.1 [27]). Finally, the maximal Lyapunov exponent computed with Rosenstein’s algorithm [28] is positive and  $\approx 1.63 \times 10^{-3}$ .

Note that in the chaotic region,  $St_5$  and  $St_6$  are both saddle-foci. The corresponding two-dimensional manifolds are thus respectively stable and unstable spirals. The observed chaotic kinetics corresponds to trajectories switching between these two spirals via the one-dimensional manifold of  $St_5$ . The same mechanism appears in the Willamowski–Rössler model analyzed by Aguda et al. [29].

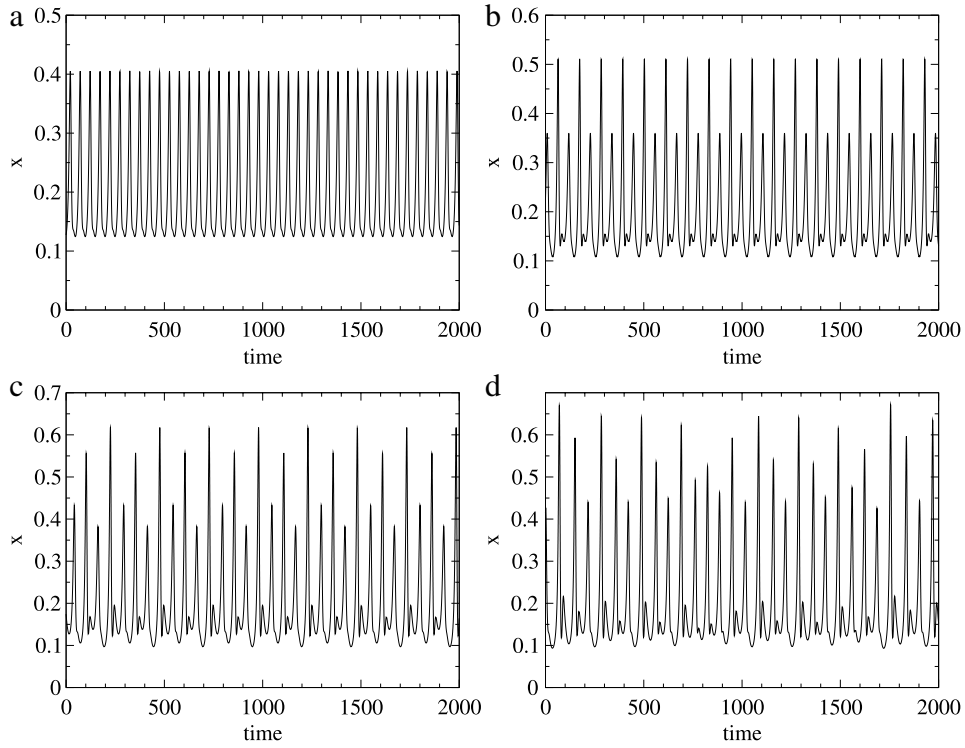


**Fig. 1.** Asymptotic behavior of  $x$  vs  $t$  for  $\alpha_1 = 0.82$  (simple oscillations – P1) (a),  $\alpha_1 = 0.80$  (biperiodic oscillations – P2) (b),  $\alpha_1 = 0.782$  (quadriperiodic oscillations – P4) and  $\alpha_1 = 0.77$  (chaos). Other parameters are  $\alpha_{-1} = 0.1$ ,  $\alpha_3 = 0.2$ ,  $\alpha_5 = 0.8$  and  $\alpha_{-5} = 0.9$  and initial conditions are  $x = y = z = 0.1$ .

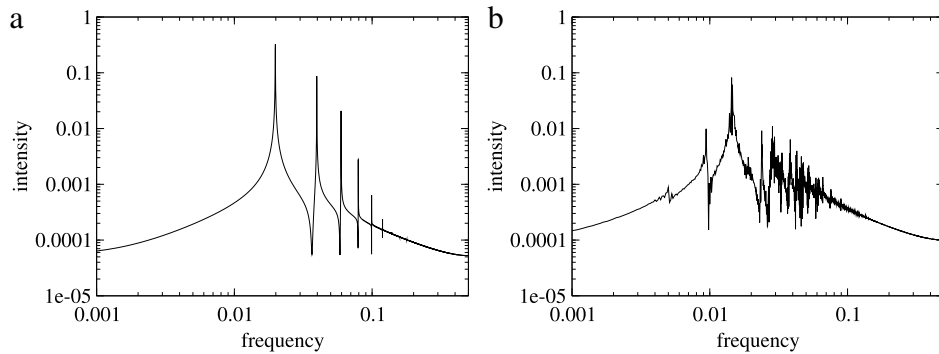


**Fig. 2.** Power spectra of  $x(t)$  for  $\alpha_1 = 0.82$  (a) and  $\alpha_1 = 0.77$  (b). Other parameters are  $\alpha_{-1} = 0.1$ ,  $\alpha_3 = 0.2$ ,  $\alpha_5 = 0.8$  and  $\alpha_{-5} = 0.9$  and initial conditions are  $x = y = z = 0.1$ .

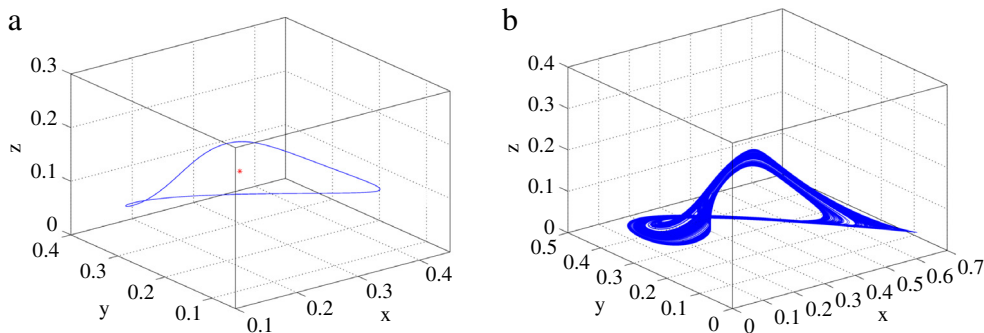


**Fig. 3.** Phase space representations for  $\alpha_1 = 0.82$  (simple oscillations) (a) and  $\alpha_1 = 0.77$  (chaos) (b).  $St_6$  is represented by the red star inside the limit cycle. Other parameters and initial conditions are the same as on Fig. 1.

Fig. 4 plots the corresponding bifurcation diagram, which shows the stationary states as well as the minima and maxima of the time-dependent solutions as a function of the parameter  $\alpha_1$ .  $St_4$  has not

been represented on the diagram, because its domain of existence is very limited for our choice of parameters. As  $\alpha_1$  decreases, the chaotic behavior appears *via* period-doubling bifurcations and

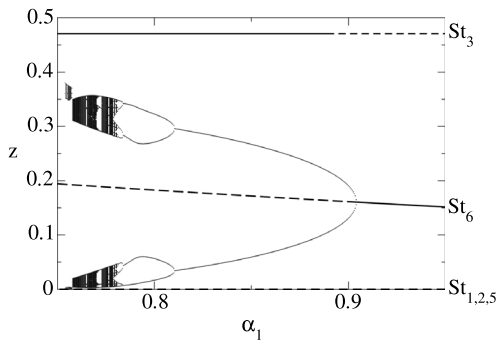


**Fig. 4.** Bifurcation diagram for the  $z$  variable. Parameters are  $\alpha_{-1} = 0.1$ ,  $\alpha_3 = 0.2$ ,  $\alpha_5 = 0.8$  and  $\alpha_{-5} = 0.9$ . Continuous and dashed lines represent stable and unstable steady states, respectively.

coexists with a stable stationary state ( $St_3$ ). The size of the chaotic attractor increases as  $\alpha_1$  is further reduced, which finally results in a collision between this attractor and one of the steady states and consequently in a disappearance of chaotic trajectories.

To summarize, the number of steady states is the same in the original and the extended models and chaos appears through the same type of mechanism. Confinement does not induce new type of instabilities but, as additional numerical investigations show, changes slightly the size of the basin of attraction of the different states and displaces the bifurcation points. Confinement seems to play only a minor role in the deterministic behavior of the extended Willamowski–Rössler model, which thus behaves qualitatively like the original (unconfined) one. In the next section, we analyze to what extent fluctuations influence the dynamics and the interactions between the chaotic trajectories and the stationary states.

#### 4. Stochastic dynamics

We performed stochastic simulations of the extended Willamowski–Rössler model presented above to assess the role played by intrinsic (internal) fluctuations of composition on the robustness of the chaotic dynamics. We first discuss the case of homogeneous fluctuations.

##### 4.1. Fluctuations in a homogeneous system

We used the Gillespie algorithm [30,31], which is an off-lattice stochastic simulation method where the system is considered to be perfectly stirred. This algorithm relies on the use of extensive propensity functions and thus on the definition of an extensivity parameter, which we chose to be the total number of boxes in the system ( $N_0$ ). The algorithm is detailed in Appendix A.

Similarly to what has been reported for other chaotic models, we observe that the presence of steady states can strongly affect the dynamics of the chaotic regime in the presence of fluctuations. Generally speaking, the parametric domain where chaos can be found is greatly reduced with respect to the mean-field case. A simple dynamics, corresponding to a relaxation to one of the absorbing states, is observed for most of the parameter values where chaos should be found in view of the deterministic predictions. This behavior is seen in small as well as in large systems (up to  $N_0 = 10^7$ ) and the final state in which the system ends up often depends on its size. A typical example of such a relaxation is given in Fig. 5, where the deterministic behavior is also shown for comparison. When the amplitude of the strange attractor is small and for sufficiently large systems, chaos is observed but only for finite times: the system eventually reaches one of the absorbing steady states mentioned above and remains

**Table 1**

Typical behavior of the system in function of its size ( $N_0$ ) and the particles' mobility ( $\Gamma$ ). SSt: stationary state, ASt: absorbing state.

	$\Gamma = 1$	$\Gamma = 10$	$\Gamma = 100$	$\Gamma = 1000$	Gillespie
$300 \times 300$	SSt	SSt	Oscillations	Chaos	Chaos
$100 \times 100$	SSt	SSt	Chaos	ASt	ASt
$50 \times 50$	SSt	SSt	ASt	ASt	ASt
$10 \times 10$	ASt	ASt	ASt	ASt	ASt

there indefinitely. Examples of these transient chaotic kinetics are given in Fig. 6, for two different system sizes and Fig. 7 depicts a case where chaos possesses a longer lifetime.

The disappearance of chaos can be traced back to the fact that most chaotic trajectories come very close to one of the steady states. Even fluctuations of very small amplitude can induce a collision with these states, which results in the disappearance of chaos. We should thus expect chaos to be observed in homogeneous systems only in the limit where  $N_0 \rightarrow \infty$ . Spatial confinement thus plays an important role in the homogeneous stochastic dynamics. The proximity of chaotic trajectories and steady states that leads to the disappearance of chaos is indeed due to the confined character of phase space, which is itself a consequence of having  $x + y + z \leq 1$  at all times. We now turn to the role played by inhomogeneous fluctuations.

##### 4.2. Inhomogeneous fluctuations

To assess the role of inhomogeneous fluctuations of composition, lattice kinetic Monte Carlo (KMC) simulations were performed. We used square lattices whose nodes either contain a single particle or are empty. In addition to the reactive processes considered so far, the mobility of the particles needs to be included explicitly in the stochastic description of the system. As explained in more detail in Appendix B, we did so by adding a process corresponding to the hopping of particles to neighboring empty nodes. This additional process is characterized by a jump probability per time unit,  $\Gamma$ . In this work, we considered that all the species have the same hopping probability and we consequently set  $\Gamma_X = \Gamma_Y = \Gamma_Z = \Gamma$ .

We varied two parameters: the size of the system ( $N_0$ ) and the mobility of particles ( $\Gamma$ ). Based on the results from the previous section, the kinetic parameters were selected such that the chaotic attractor is compact and occupies a central position in phase space, in order to minimize the interactions with the absorbing states and to maximize the probability of observing chaotic dynamics. Table 1 summarizes the results of the spatially extended simulations. We were able to distinguish between 4 qualitatively different behaviors: absorbing states, stationary states, oscillations and chaos. We discuss below the emergence of these different dynamics and the transitions between them.

When diffusion is fast enough, the trajectories are similar those obtained with the Gillespie simulations for similar size and chaotic behaviors are thus destroyed in favor of absorbing states. For instance, with a system of  $N_0 = 2.5 \times 10^3$  sites (a  $50 \times 50$  lattice), a hopping probability per unit time  $\Gamma = 100$  is sufficient to induce a transition of chaotic trajectories to an absorbing state (ASt). Since they are more readily mixed, small systems (say, a  $10 \times 10$  lattice) reach absorbing states for lower mobilities ( $\Gamma = 1$  being here sufficient). These result further confirm the destructive role that homogeneous fluctuations of composition have in the emergence of chaos.

For very slow diffusion, chaos is usually lost as well, regardless of the size of the system. We observe that the molar fractions instead first fluctuate around a “pseudo-stationary” state with non-vanishing values, before eventually switching to an absorbing state. For example, Fig. 8 depicts a case where the composition

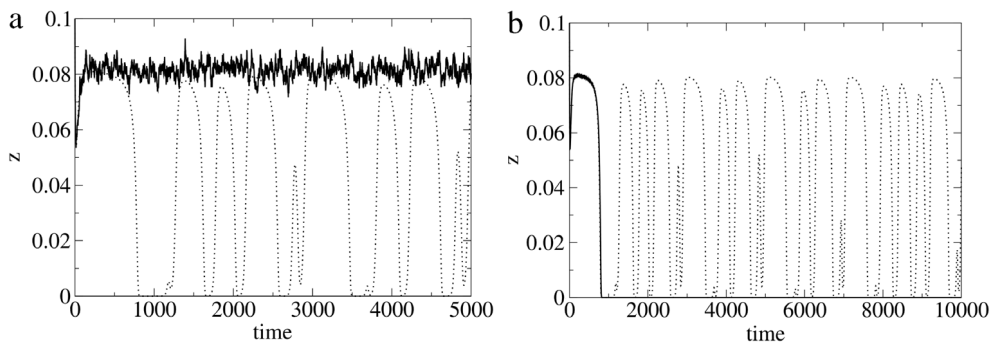


**Fig. 5.** Stochastic (plain curves) and deterministic (dotted lines) time series of  $z$  for  $\alpha_1 = 0.093$ ,  $\alpha_{-1} = 0.12$ ,  $\alpha_3 = 0.03$ ,  $\alpha_5 = 0.08$  and  $\alpha_{-5} = 0.9$ . Initial conditions are  $x = y = z = 0.1$ . In Fig. 5(a) the system size is  $N_0 = 10^4$  and the trajectory ends up in state  $St_3$ , while in Fig. 5(b),  $N_0 = 10^7$  and the state  $St_2$  is reached for long times.

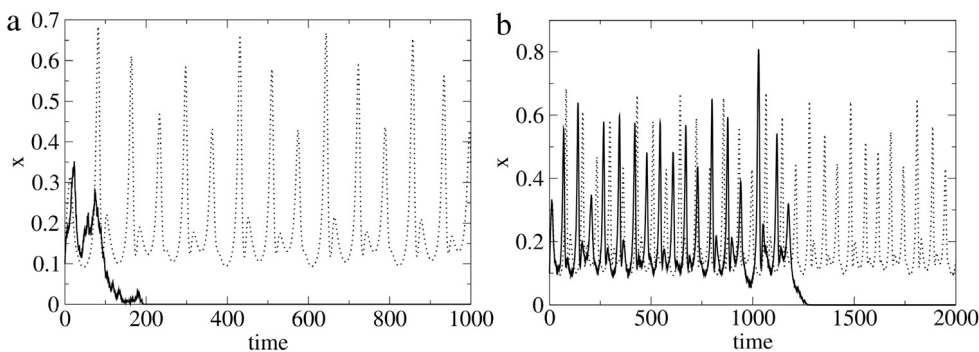


**Fig. 6.** Stochastic (plain curves) and deterministic (dotted lines) trajectories of  $x$ . In this case,  $\alpha_1 = 0.77$ ,  $\alpha_{-1} = 0.1$ ,  $\alpha_3 = 0.2$ ,  $\alpha_5 = 0.8$  and  $\alpha_{-5} = 0.9$  and initial conditions are  $x = y = z = 0.1$ . The system size is  $N_0 = 10^3$  in Fig. 6(a) and  $10^4$  in Fig. 6(b). In each case, the steady state  $St_3$  is eventually reached.

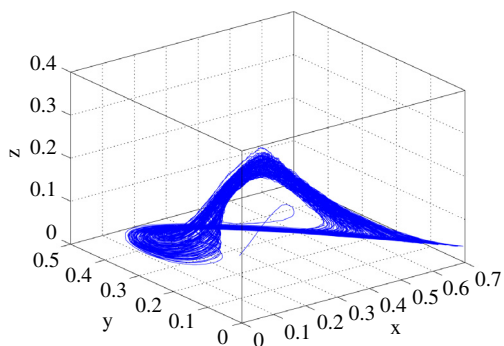


**Fig. 7.** Stochastic trajectory in the phase space for  $\alpha_1 = 0.77$ ,  $\alpha_{-1} = 0.1$ ,  $\alpha_3 = 0.2$ ,  $\alpha_5 = 0.8$  and  $\alpha_{-5} = 0.9$  and initial conditions are  $x = y = z = 0.1$ . The size of the system is  $N_0 = 9 \times 10^4$ .

fluctuates around  $(0.27, 0.23, 0.078)$  before settling on  $(0.27, 0.30, 0)$ . The lifetime of these pseudo-steady state (denoted as  $Sst$  in Table 1) increases with the size of the system. Note that the chemical composition of the low-mobility steady states reached in this way differs from that of the states predicted by the deterministic approach. The destruction of complex dynamics (such as oscillations) and the displacement of steady states have already been reported in previous works on chemical dynamics on lattices (see Section 1). These deviations have been traced back to the presence of strong short-range spatial correlations, which arise thanks to a combination of the low dimensionality of the support, of the nonlinearity of the reactive processes and of the low mobility of particles. We reach a similar conclusion, as simulations show that the first-neighbors spatial correlations of the different species are always large in the limit of low mobility hereby considered.

More surprisingly, we also observed that chaos can be gradually re-obtained for *intermediate* mobilities. To illustrate this, we plot in Fig. 9 the phase space trajectories obtained with different

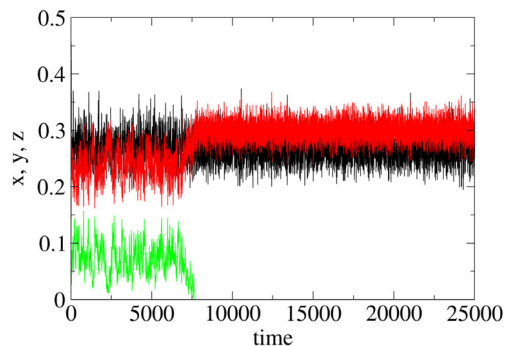


**Fig. 8.** Stochastic trajectories of  $x$  (black),  $y$  (red) and  $z$  (green) for a system size  $N_0 = 2.5 \times 10^3$  and a mobility  $\Gamma = 1$ . The other parameters are  $\alpha_1 = 0.77$ ,  $\alpha_{-1} = 0.1$ ,  $\alpha_3 = 0.2$ ,  $\alpha_5 = 0.8$  and  $\alpha_{-5} = 0.9$  and initial conditions are  $x = y = z = 0.1$ . (For interpretation of the references to color in this figure legend, the reader is referred to the web version of this article.)

mobilities for a  $100 \times 100$  system. For slow diffusion, the composition of the system fluctuates around a pseudo steady-state, as explained above (Fig. 9(a)). As we increase  $\Gamma$ , the fluctuations of composition around this stationary state first seem to be amplified and become more and more regular. For a small range of  $\Gamma$ , it is possible to observe damped oscillations sustained by fluctuations, which is a frequently reported phenomenon in the neighborhood of a Hopf bifurcation in noisy oscillating systems. As the mobility is further increased, these changes translate in an unfolding of the corresponding attractor, which takes the form of a noisy cycle (Fig. 9(b)). For large enough (but not too high) mobilities, this cycle gradually bends to give a manifold resembling the deterministic chaotic attractor, as can be seen in Figs. 9(c) and 9(d). The chaotic character of the dynamics can be confirmed with Fourier power spectra of the autocorrelation function of the time series, which show strong similarities with those of

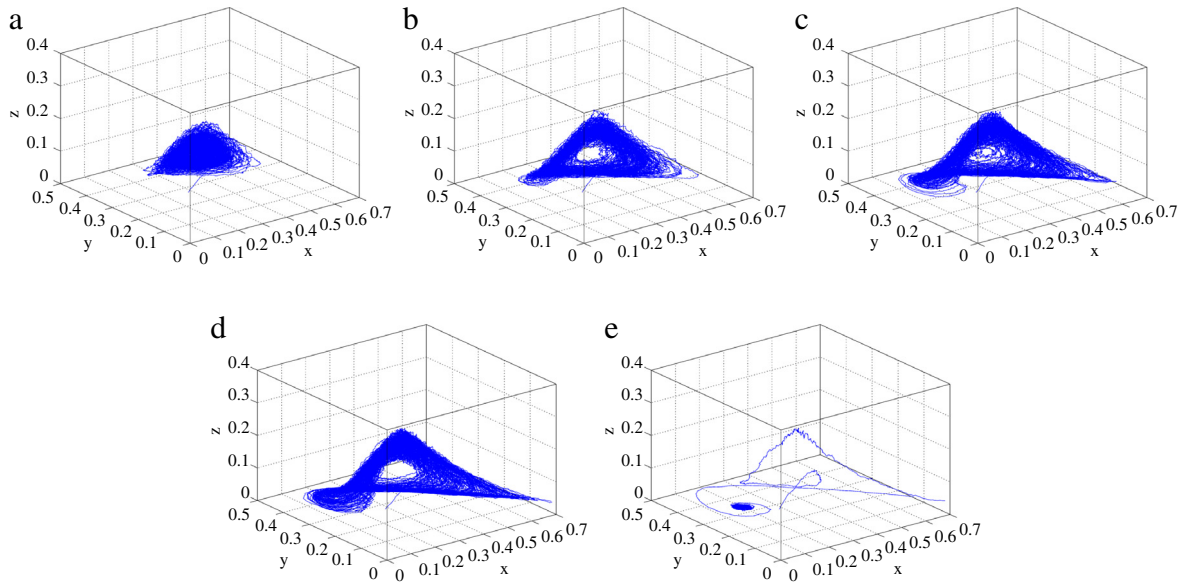


**Fig. 9.** Phase representations in a  $100 \times 100$  system with  $\Gamma = 25$  (a),  $\Gamma = 50$  (b),  $\Gamma = 75$  (c),  $\Gamma = 100$  (d) and  $\Gamma = 1000$  (e). The other parameters are  $\alpha_1 = 0.77$ ,  $\alpha_{-1} = 0.1$ ,  $\alpha_3 = 0.2$ ,  $\alpha_5 = 0.8$  and  $\alpha_{-5} = 0.9$  and initial conditions are  $x = y = z = 0.1$ .

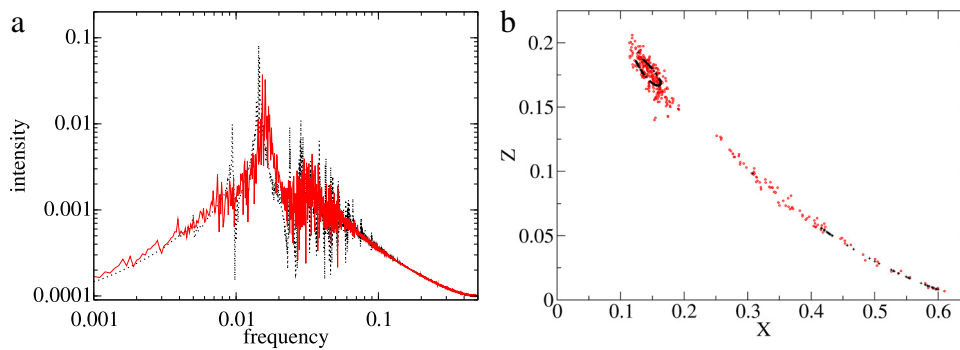


**Fig. 10.** Power spectra and section in a  $100 \times 100$  system with  $\Gamma = 100$ . On Fig. 10(a), the stochastic spectrum (red line) is compared to the deterministic curve (black dotted line). On Fig. 10(b), the section is taken across the phase representation along plane  $y = 0.2$ . Black dots represent the deterministic data while red circles correspond to the stochastic section. The other parameters are the same as on Fig. 9.

the corresponding deterministic signals (Fig. 10(a)). Moreover, sections taken across the attractor show a dispersion of points along lines, which is a typical signature of chaos (Fig. 10(b)). These sections are also qualitatively similar to the ones obtained by numerical integration of the deterministic equations. The chaotic trajectories disappear abruptly for larger mobilities and the dynamics of Gillespie simulations (leading to an absorbing steady state) is re-obtained, as expected.

In larger systems (e.g.  $300 \times 300$  lattice), the transition from oscillations (Fig. 11(a)) to chaos (Fig. 11(b)) appears even more clearly. When oscillations are obtained in simulations, a dominating frequency and the corresponding subharmonics can distinctly be identified in the power spectrum presented in Fig. 11(c), where we also plotted the corresponding chaotic deterministic spectrum for comparison. When increasing  $\Gamma$ , the spectrum gradually transforms into a continuum of peaks at incommensurate frequencies characteristic of chaotic trajectories (Fig. 11(d)). This transition is also reflected in the cross sections of the attractors, for which we observe that the clouds of dots in Fig. 11(e), which are typical of a noisy limit cycle, deform and stretch out to give lines (Fig. 11(f)).

Like before, the deviations from the deterministic behavior can be traced back to the presence of spatial correlations between particles. The intensity of the first-neighbors spatial covariance for example decreases gradually as  $\Gamma$  decreases, and as the dynamics switches from a pseudo-steady state to oscillations and to chaos.

It thus appears that the mobility of particles effectively acts as a new bifurcation parameter: increasing the hopping probability while keeping the other parameters constant has an effect on the system's behavior that is qualitatively similar to a decrease of  $\alpha_1$  in the deterministic case (see Fig. 4).

## 5. Conclusions

We have studied how fluctuations and mobility influence the chaotic behavior of an amended Willamowski-Rössler model, which takes into account the molecular crowding that characterizes small systems. We showed that because of the presence of fluctuations, the size of the system and the mobility act as two new bifurcation parameters. Varying these parameters allows one to switch from a stationary state to oscillations or to chaos, under conditions for which the deterministic equations predict that only chaos can be found. Moreover, they can be used in synergy to prevent the destruction of chaotic dynamics by the absorbing states induced by the aforementioned molecular crowding. A large system size coupled to an intermediate mobility prevents the complete consumption of the species, and thus the emergence of trivial, non-reactive dynamics. It should be noted that in this model, an efficient synchronization of the oscillations does not always prevent the system from falling into absorbing states, which is in

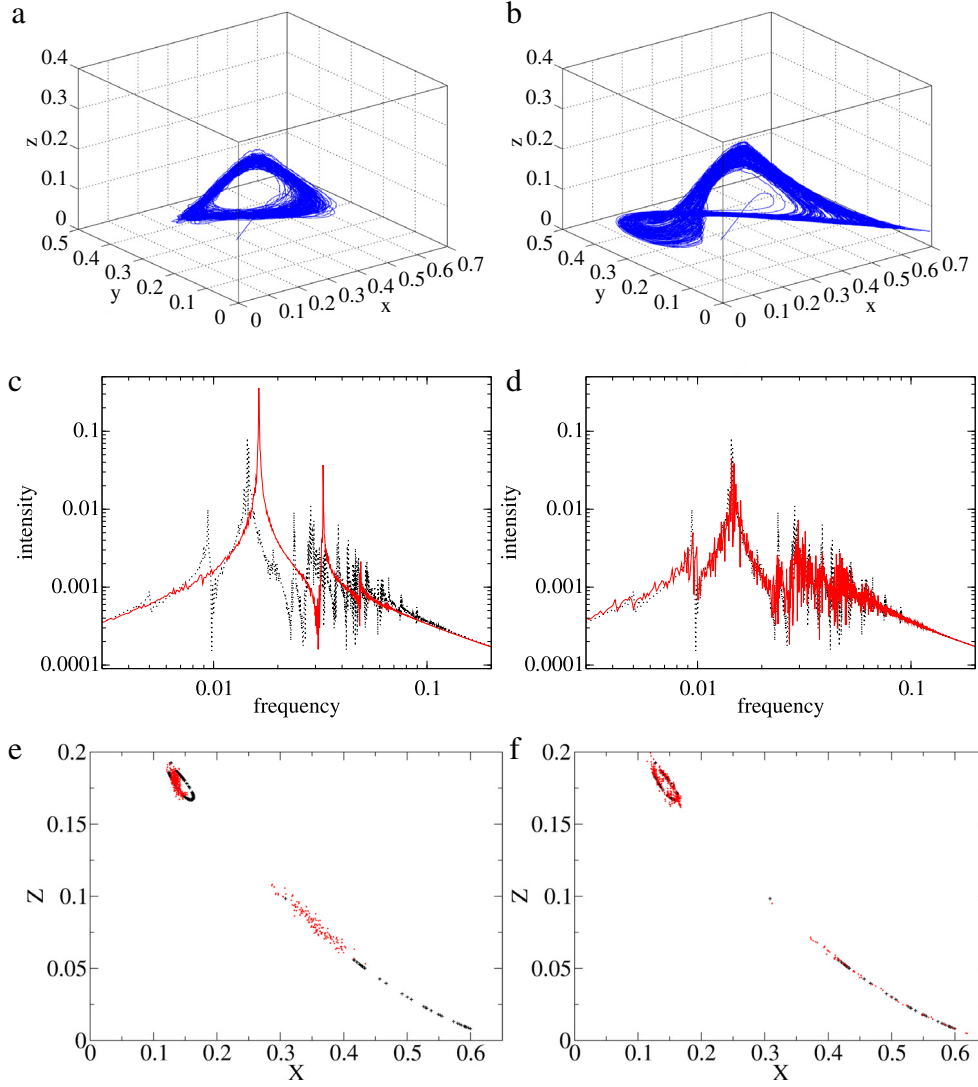


**Fig. 11.** Phase space representations, power spectra and sections taken along plane  $y = 0.2$  across the phase trajectory in a  $300 \times 300$  system. Figures (a), (c) and (e) correspond to  $\Gamma = 100$  and cases (b), (d) and (f) to  $\Gamma = 1000$ . The other parameters are the same as on Fig. 9. In Figures (c) to (f), the deterministic data are represented in black for comparison.

opposition to what has been reported for the population dynamics model analyzed by Efimov et al. [19].

In conclusion, the mean field description of this low-dimensional system correctly predicts the evolution of the chemical dynamics only in the limit of macroscopic and well-mixed systems. It breaks down for systems containing low-mobility particles and for small finite size systems, whatever the mobility. Clusters of particles generated by the inhomogeneous fluctuations of composition appear to be the main source of deviations from the mean field behavior. As we expect the sensitivity to fluctuations and to mobility to depend on the system considered, it would be appropriate to perform a similar study on different models to assess the generality of the results we present here. Other potentially compensating effects should also be investigated, such as the geometry and the dimensionality of the system, which are known to affect fluctuation-induced behaviors.

#### Acknowledgment

One of the authors (V.V.) is supported by a F.R.S.-FNRS Ph.D. fellowship.

#### Appendix A. Gillespie simulations

The Gillespie method neglects the local interactions between species but takes fluctuations into account. In this algorithm, the selection of the process  $\mu$  and the calculation of the time increment  $\Delta\tau$  involve the propensity functions  $w_\mu(\mathbf{n}) = c_\mu h_\mu(\mathbf{n})$ , where  $c_\mu$  depends on the kinetic constant of the reaction  $\mu$ ,  $\mathbf{n}$  is a vector containing the number of molecules of each species and  $h_\mu(\mathbf{n})$  gives the number of combinations formed with  $\mathbf{n}$  molecules reacting according to  $\mu$ . More precisely,  $\Delta\tau$  is given by

$$\Delta\tau = -\frac{\ln(r_1)}{w(\mathbf{n})} \quad (\text{A.1})$$

and  $\mu$  is chosen such that

$$\sum_{i=1}^{\mu-1} \frac{w_i(\mathbf{n})}{w(\mathbf{n})} < r_2 \leq \sum_{i=1}^{\mu} \frac{w_i(\mathbf{n})}{w(\mathbf{n})}, \quad (\text{A.2})$$

where  $r_1$  and  $r_2$  are random numbers and  $w(\mathbf{n})$  is the total propensity function. The propensity functions for each reaction are

given by :

$$\begin{aligned}
 w_1 &= \alpha_1 \frac{n_x (N_0 - n_x - n_y - n_z)}{N_0} \\
 w_{-1} &= \alpha_{-1} \frac{n_x (n_x - 1)}{N_0} \\
 w_2 &= \frac{n_x n_y}{N_0} \\
 w_3 &= \alpha_3 n_y \\
 w_4 &= \frac{n_x n_z}{N_0} \\
 w_5 &= \alpha_5 \frac{n_z (N_0 - n_x - n_y - n_z)}{N_0} \\
 w_{-5} &= \alpha_{-5} \frac{n_z (n_z - 1)}{N_0}, \tag{A.3}
 \end{aligned}$$

where  $N_0$  corresponds to the size of the system.

## Appendix B. Spatial KMC simulations

In the spatial KMC method, we consider an  $L \times L$  lattice composed of  $N_0$  sites of coordinates  $\mathbf{R}$ , characterized by a local occupation number  $\mathcal{s}_\gamma(\mathbf{R}, t)$ . This number is defined as follows :

$$\begin{aligned}
 \mathcal{s}_\gamma(\mathbf{R}, t) &\equiv \begin{cases} 1, & \text{if the site } \mathbf{R} \text{ is occupied by species } \gamma \text{ at time } t \\ 0, & \text{if the site } \mathbf{R} \text{ is not occupied by species } \gamma \text{ at time } t. \end{cases} \tag{B.1}
 \end{aligned}$$

The ensemble of these variables,  $\mathcal{s}(t) \equiv \{\mathcal{s}_\gamma(\mathbf{R}, t)\}$ , defines the instantaneous microscopic configuration of the system. The *intrinsic probability* associated to a chemical reaction is proportional to its kinetic constant. In the case of a diffusion process, we introduce a jump probability,  $\Gamma$ , related to the mobility of the particles. The probabilities are given by:

$$\begin{aligned}
 p_X &= \frac{\Gamma_X}{k_{tot}} & p_Y &= \frac{\Gamma_Y}{k_{tot}} & p_Z &= \frac{\Gamma_Z}{k_{tot}} \\
 p_1 &= \frac{\alpha_1}{k_{tot}} & p_{-1} &= \frac{\alpha_{-1}}{k_{tot}} & p_2 &= \frac{\alpha_2}{k_{tot}} = \frac{1}{k_{tot}} \\
 p_3 &= \frac{\alpha_3}{k_{tot}} & p_4 &= \frac{\alpha_4}{k_{tot}} = \frac{1}{k_{tot}} & p_5 &= \frac{\alpha_5}{k_{tot}} \\
 & & p_{-5} &= \frac{\alpha_{-5}}{k_{tot}}, \tag{B.2}
 \end{aligned}$$

where  $k_{tot} = \Gamma_X + \Gamma_Y + \Gamma_Z + \alpha_1 + \alpha_{-1} + \alpha_2 + \alpha_3 + \alpha_4 + \alpha_5 + \alpha_{-5}$ . At every time, a site, a first-neighbor and a process are randomly selected. Process  $I$  is selected if :

$$\sum_{i=1}^{I-1} p_i < r \leq \sum_{i=1}^I p_i, \tag{B.3}$$

where  $p_i$  corresponds to one of the reaction probabilities given in (B.2) and  $r$  is a random number. The process occurs if it is compatible with  $\mathcal{s}(t)$ :

- For the *diffusion* of species  $\gamma$  ( $\gamma \equiv X, Y$  or  $Z$ ), the algorithm selects a pair of adjacent sites, where one of the two has to contain the species  $\gamma$  and the other one has to be empty. If this condition is satisfied, species  $\gamma$  moves to the empty site.
- For the *direct reaction* (11), if site  $\mathbf{R}$  contains  $X$  and if the chosen neighbor is an empty site, the reaction occurs and both sites subsequently contain an  $X$  particle.
- For the *reverse reaction* (11), if site  $\mathbf{R}$  contains  $X$ , and so does its randomly picked neighbor, the  $X$  particle leaves the site  $\mathbf{R}$ .
- For *reaction* (12), if site  $\mathbf{R}$  contains  $X$  and if the selected neighbor contains  $Y$ ,  $X$  is converted into  $Y$ .
- For *reaction* (13), if site  $\mathbf{R}$  contains  $Y$ , this site becomes empty.
- For *reaction* (14), if site  $\mathbf{R}$  contains  $X$  and that the selected neighbor contains  $Z$ , both sites become empty.
- For the *direct reaction* (14), if site  $\mathbf{R}$  contains  $Z$  and the adjacent site is free, a  $Z$  particle forms on the formerly empty site.
- For the *reverse reaction* (14), if site  $\mathbf{R}$  contains  $Z$  and so does the selected neighbor, the  $Z$  particle disappears from site  $\mathbf{R}$ .

If the instantaneous configuration is not compatible with the selected process, the lattice is not modified. In both cases, the time is incremented by a Monte Carlo Step (MCS) :

$$\Delta\tau = \frac{1}{k_{tot} N_0}, \tag{B.4}$$

where  $\Delta\tau$  represents the duration of an MCS in the adimensional time used in the lattice Willamowski–Rössler model.

## References

- [1] A. Ostafin, *Nanoreactor Engineering for Life Sciences and Medicine*, Artech House, Boston, 2009.
- [2] M. Yoshizawa, J.K. Klosterman, M. Fujita, *Angew. Chem., Int. Ed.* 48 (2009) 3418.
- [3] C. Sachs, M. Hildebrand, S. Völkening, J. Winterlin, G. Ertl, *Science* 293 (2001) 1635.
- [4] V. Johánek, M. Laurin, A.W. Grant, B. Kasemo, C.R. Henry, J. Libuda, *Science* 304 (2004) 1639.
- [5] Y. De Decker, F. Baras, *Eur. Phys. J. B* 78 (2010) 173.
- [6] R.F. Fox, J. Keizer, *Phys. Rev. A: At. Mol. Opt. Phys.* 43 (1991) 1709.
- [7] G. Nicolis, V. Balakrishnan, *Phys. Rev. A: At. Mol. Opt. Phys.* 46 (1992) 3569.
- [8] P. Geysmans, G. Nicolis, *J. Chem. Phys.* 99 (1993) 8964.
- [9] Q. Li, H. Wang, *Phys. Rev. E* (3) 58 (1998) R1191.
- [10] X.-G. Wu, R. Kapral, *Phys. Rev. Lett.* 70 (1993) 1940.
- [11] X.-G. Wu, R. Kapral, *J. Chem. Phys.* 100 (1994) 5936.
- [12] R. Kapral, X.-G. Wu, *J. Phys. Chem.* 100 (1996) 18976.
- [13] D. Fanelli, A.J. McKane, *Phys. Rev. E* (3) 82 (2010) 021113.
- [14] A. Provata, J.W. Turner, G. Nicolis, *J. Stat. Phys.* 70 (1993) 1195.
- [15] A. Tretyakov, A. Provata, G. Nicolis, *J. Phys. Chem.* 99 (1995) 2770.
- [16] S. Prakash, G. Nicolis, *J. Stat. Phys.* 82 (1996) 297.
- [17] S. Prakash, G. Nicolis, *J. Stat. Phys.* 86 (1997) 1289.
- [18] A. Provata, G. Nicolis, F. Baras, *J. Chem. Phys.* 110 (1999) 8361.
- [19] A. Efimov, A. Shabunin, A. Provata, *Phys. Rev. E* (3) 78 (2008) 056201.
- [20] A.V. Shabunin, F. Baras, A. Provata, *Phys. Rev. E* (3) 66 (2002) 036219.
- [21] D. Bullara, Y. De Decker, *Nature Commun.* 6 (2015) 6971.
- [22] A.J. McKane, T.J. Newman, *Phys. Rev. Lett.* 94 (2005) 218102.
- [23] C.A. Lugo, A.J. McKane, *Phys. Rev. E* (3) 78 (2008) 051911.
- [24] T. Biancalani, T. Galla, A.J. McKane, *Phys. Rev. E* (3) 84 (2011) 026201.
- [25] N. Kouvaris, D. Kugiumtzis, A. Provata, *Phys. Rev. E* (3) 84 (2011) 036211.
- [26] K.-D. Willamowski, O.E. Rössler, *Z. Nat.forsch. A* 35a (1980) 317.
- [27] R. Hegger, H. Kantz, T. Schreiber, *Chaos* 9 (1999) 413.
- [28] M.T. Rosenstein, J.J. Collins, C.J. De Luca, *Physica D* 65 (1993) 117.
- [29] B.D. Aguda, B.L. Clarke, *J. Chem. Phys.* 89 (1988) 7428.
- [30] D.T. Gillespie, *J. Comput. Phys.* 22 (1976) 403.
- [31] D.T. Gillespie, *J. Phys. Chem.* 81 (1977) 2340.